

# Compressional and shear wave properties of marine sediments: Comparisons between theory and data

Michael J. Buckingham<sup>a)</sup>

Marine Physical Laboratory, Scripps Institution of Oceanography, University of California, San Diego, 9500 Gilman Drive, La Jolla, California 92093-0238

(Received 7 June 2004; accepted for publication 26 August 2004)

According to a recently developed theory of wave propagation in marine sediments, the dispersion relationships for the phase speed and attenuation of the compressional and the shear wave depend on only three macroscopic physical variables: porosity, grain size, and depth in the sediment. The dispersion relations also involve three (real) parameters, assigned fixed values, representing microscopic processes occurring at grain contacts. The dispersion relationships are compared with extensive data sets, taken from the literature, covering the four wave properties as functions of all three physical variables. With no adjustable parameters available, the theory matches accurately the trends of all the data sets. This agreement extends to the compressional and shear attenuations, in that the theory accurately traces out the *lower bound* to the widely distributed measured attenuations: the theory predicts the *intrinsic* attenuation, arising from the irreversible conversion of wave energy into heat, whereas the measurements return the *effective* attenuation, which includes the intrinsic attenuation plus additional sources of loss such as scattering from shell fragments and other inhomogeneities in the medium. Provided one wave or physical property is known, say the compressional speed or the porosity, all the remaining sediment properties may be reliably estimated from the theory. © 2005 Acoustical Society of America. [DOI: 10.1121/1.1810231]

PACS numbers: 43.30.Ma [AIT]

Pages: 137–152

## I. INTRODUCTION

Over recent decades, extensive data sets have been published by Hamilton *et al.*<sup>1–8</sup> and Richardson *et al.*<sup>9–12</sup> on the wave properties of surficial, unconsolidated marine sediments. It is evident from the data that an unconsolidated sediment is capable of supporting two types of propagating wave, a compressional (longitudinal) wave and a much slower shear (transverse) wave. Although there have been several attempts to detect a third type of wave, the “slow” compressional wave of the Biot theory,<sup>13,14</sup> all have returned a negative result, including the most recent experiment by Simpson *et al.*<sup>15</sup> Based on this evidence, it is tacitly assumed throughout the following discussion that the slow wave in an unconsolidated sediment is negligible if not absent altogether.

It is well established from the published data that the phase speed and the attenuation of both the compressional and shear wave depend, in a more or less systematic way, on the physical properties of the sediment, principally the porosity, the bulk density, the mean grain size, and the depth beneath the seafloor. Indeed, both Hamilton<sup>3,7,16</sup> and Richardson<sup>9,11,12</sup> have developed a set of empirical regression equations, each one of which expresses a wave property (e.g., the compressional phase speed) in terms of a physical property of the medium (e.g., the porosity).

Although regression equations can be satisfactorily fitted to the data, thus providing a useful predictive tool, they give little insight into the physical mechanisms underlying the

observed inter-relationships between wave parameters and physical properties. To achieve an understanding of the observed dependencies, it is necessary to turn to a theoretical model of wave propagation in the medium and, in particular, to the dispersion relationships predicted by the model. Such a model has recently been developed by Buckingham<sup>17</sup> on the basis of a specific form of dissipation arising at grain-to-grain contacts. This grain-shearing (G-S) model is intended to represent wave propagation in an unconsolidated granular medium, that is to say, a material in which the mineral grains are in contact but unbonded. By definition, this condition is taken to mean that the mineral matrix has no intrinsic strength or, equivalently, that the elastic (bulk and shear) frame moduli are identically zero.

The absence of an elastic frame in the G-S model contrasts with the starting assumption in Biot's classic theory<sup>13,14</sup> of wave propagation in porous media. Biot treated the medium as though it possessed an elastic mineral frame, an essential assumption in his analysis since the elasticity is the means by which a shear wave is supported in his model. In the G-S model, on the other hand, it is not necessary to postulate the existence of an elastic frame because elastic-type behavior emerges naturally from the analysis as a result of the intergranular interactions themselves: grain-to-grain sliding introduces a degree of rigidity into the medium, which, amongst other effects, automatically leads to the support of a shear wave. The lack of elastic (bulk and shear) frame moduli in the G-S model is consistent with the commonplace observations that an unconfined pile of sand grains shows no resistance to deformation (indicating no restoring force) and that sand grains may be picked off a pile (indicating no tensile strength). Moreover, even though the grains

<sup>a)</sup>Also affiliated with the Institute of Sound and Vibration Research, The University, Southampton SO17 1BJ, England. Electronic mail: mjb@mpl.ucsd.edu

remain unbonded, loose sand in a container shows increasing resistance to penetration (shear strength), which can only arise from intergranular interactions. Such interactions form the essence of the G-S wave-propagation model.<sup>17</sup>

The purpose of this article is to compare the theoretical properties of compressional and shear waves in marine sediments, as expressed in the dispersion relationships of the G-S model, with an extensive set of data culled from the open literature. Most of the data examined here were obtained from *in situ* measurements in siliclastic sediments.

Besides frequency, the G-S dispersion expressions for the phase speed and attenuation depend explicitly on the mean grain size, the porosity, the bulk density (which is strongly correlated with the porosity and hence is not an independent variable), and the overburden pressure (which translates into depth in the sediment). In addition, the G-S dispersion relationships involve three unknown constants which characterize the microscopic processes that occur as adjacent grains slide against one another during the passage of a wave. Once the numerical values of these three constants have been determined, by comparison with three spot-frequency data points, all the functional dependencies of the G-S theory may be evaluated and compared with the data. Thus, the predicted relationships between wave properties (e.g., shear speed) and physical properties (e.g., depth in sediment) may be compared directly with the corresponding data sets that have appeared in the literature. Such comparisons are examined in some detail in this article, along with the dispersion curves (i.e., phase speeds and attenuations versus frequency) predicted by the G-S theory, which are shown to match the available data over wide frequency ranges.

## II. THE G-S DISPERSION RELATIONS

According to Buckingham,<sup>17</sup> the compressional-wave speed,  $c_p$ , and attenuation,  $\alpha_p$ , are given by the expressions

$$c_p = \frac{c_o}{\operatorname{Re} \left[ 1 + \frac{\gamma_p + (4/3)\gamma_s}{\rho_o c_o^2} (j\omega T)^n \right]}^{-1/2}, \quad (1)$$

and

$$\alpha_p = -\frac{\omega}{c_o} \operatorname{Im} \left[ 1 + \frac{\gamma_p + (4/3)\gamma_s}{\rho_o c_o^2} (j\omega T)^n \right]^{-1/2}, \quad (2)$$

where  $j = \sqrt{-1}$ . The corresponding expressions for the shear-wave speed,  $c_s$ , and attenuation,  $\alpha_s$ , are

$$c_s = \sqrt{\frac{\gamma_s}{\rho_o}} \frac{(\omega T)^{n/2}}{\cos\left(\frac{n\pi}{4}\right)}, \quad (3)$$

and

$$\alpha_s = \omega \sqrt{\frac{\rho_o}{\gamma_s}} (\omega T)^{-n/2} \sin\left(\frac{n\pi}{4}\right). \quad (4)$$

Between them, Eqs. (1)–(4) constitute the dispersion relationships predicted by the G-S theory. Both dispersion pairs are causal, satisfying the Kramers–Kronig relationships.

Several familiar parameters appear in the G-S dispersion expressions: the angular frequency,  $\omega$ , the bulk density of the medium,  $\rho_o$ , the sound speed in the absence of grain-to-grain interactions,  $c_o$ , and an arbitrary time  $T = 1$  s, introduced solely to avoid awkward dimensions that would otherwise arise when the frequency is raised to a fractional power.

Less familiar are the three remaining parameters,  $\gamma_p$ ,  $\gamma_s$ , and the (positive, fractional) index  $n$ , which between them represent the effects of grain-to-grain interactions on the wave speeds and attenuations. From the way that they appear in the dispersion relations, and the fact that they have dimensions of pressure, it is evident that the two (real) parameters  $\gamma_p$  and  $\gamma_s$  are compressional and shear moduli, respectively, providing a measure of the normal and tangential stresses associated with intergranular sliding. In fact,  $\gamma_p$  and  $\gamma_s$  are closely analogous to the Lamé parameters of elasticity theory. There is no such analogy, however, for the dimensionless index  $n$ , which is a measure of the degree of strain hardening that is postulated to occur at intergranular contacts as grain-to-grain sliding progresses. Details of the intergranular sliding and strain-hardening mechanisms may be found in Buckingham.<sup>17</sup>

If  $n$  were zero, the compressional and shear attenuations would both vanish and the expressions for the two wave speeds would be independent of frequency. Of course, dissipation is never completely absent, so  $n$  is always finite, but it is small compared with unity, taking a value close to 0.1 for a typical sand sediment. With such a low value for  $n$ , the two G-S expressions for the wave speeds exhibit logarithmic dispersion, at levels of the order of 1% (compressional) and 10% (shear) per decade of frequency, and the associated attenuations both scale essentially as the first power of frequency,  $f$ . These simple frequency-dependencies derive directly from straightforward approximations<sup>17</sup> for the exact expressions in Eqs. (1)–(4).

From the point of view of wave propagation, two important physical properties of sediments are the porosity,  $N$ , and the mean grain diameter,  $u_g$ . In addition, the intergranular interactions, and hence also the wave properties, are sensitive to the overburden pressure, which scales with the depth,  $d$ , in the sediment. All three parameters appear in the G-S dispersion relations, the porosity through  $c_o$  and  $\rho_o$ , while the grain size and the depth in the sediment, both raised to fractional powers, appear in the expressions given below for  $\gamma_p$  and  $\gamma_s$ . These two moduli also show a weak but significant dependence on the porosity,  $N$ .

It is well known that the bulk density,  $\rho_o$ , may be expressed in terms of the porosity as a weighted mean of the density of the pore water,  $\rho_w$  and the density of the mineral grains,  $\rho_g$

$$\rho_o = N\rho_w + (1-N)\rho_g. \quad (5)$$

Similarly, the bulk modulus of the medium,  $\kappa_o$ , may be expressed in terms of the porosity as a weighted mean

$$\frac{1}{\kappa_o} = N \frac{1}{\kappa_w} + (1-N) \frac{1}{\kappa_g}, \quad (6)$$

where  $\kappa_w$  and  $\kappa_g$  are the bulk moduli of the pore water and the mineral grains, respectively. If the sediment were a simple suspension in which grain-to-grain interactions were absent, the speed of sound would be  $c_o$ , which depends on the porosity through Wood's equation<sup>18</sup>

$$c_o = \sqrt{\frac{\kappa_o}{\rho_o}}. \quad (7)$$

In the limit of low frequency, the G-S expression for the compressional wave speed in Eq. (1) reduces to  $c_o$ , while Eqs. (2)–(4) show that  $\alpha_p$ ,  $c_s$ , and  $\alpha_s$  all approach zero. Thus, according to the G-S dispersion relations, in the low-frequency limit, the effects of grain-to-grain interactions are negligible and the medium acts as a simple suspension.

Turning to the compressional and shear moduli,  $\gamma_p$  and  $\gamma_s$ , their dependencies on grain size, depth in the sediment, and porosity are established by treating the mineral grains as elastic spheres, which deform slightly under the influence of the overburden pressure. At the point where two grains touch, a small, tangential circle of contact is formed, the radius of which is given by the Hertz theory<sup>19</sup> of elastic bodies in contact. Assuming that the two grains are identical spheres of diameter  $u_g$ , Young's modulus  $E_g$  and Poisson's ratio  $\theta_g$ , the radius,  $a$ , of the circle of contact is

$$a = \sqrt[3]{\frac{3}{8} F \frac{(1 - \theta_g^2)}{E_g} u_g}, \quad (8)$$

where  $F$  is the force pressing the spheres together. At depth  $d$  in the sediment, the force  $F$  scales with the overburden pressure,  $P$ , which is defined<sup>20</sup> as the excess pressure arising from the difference between the bulk density of the sediment and the density of the pore water

$$P = (\rho_o - \rho_w)gd = (1 - N)(\rho_g - \rho_w)gd, \quad (9)$$

where  $g$  is the acceleration due to gravity. The expression on the right of Eq. (9) derives from Eq. (5) for the bulk density, which accounts for the dependence of the overburden pressure on the porosity. It follows that the radius of the circle of contact may be expressed as

$$a \propto [(1 - N)du_g]^{1/3}, \quad (10)$$

where the constant of proportionality involves the elastic properties of the mineral grains but is independent of the bulk properties of the two-phase medium.

Now, the moduli  $\gamma_p$  and  $\gamma_s$  scale with the rates at which sliding events occur within the circle of contact of radius  $a$ . With many micro-asperities distributed randomly over each face of the contact area, the rate of sliding will scale with the number of asperities available to slip against one another. In the case of the compressional modulus, most of the sliding takes place around the perimeter of the circle of contact, where the normal pressure is a minimum. Thus, the number of asperities involved in the sliding process is expected to scale with the perimeter of the circle of contact, and hence  $\gamma_p$  is proportional to  $a$ . Shearing, on the other hand, involves a slip of the two flat faces of the surface of contact against each other, in which case the number of available asperities scales with area of the circle of contact, and therefore  $\gamma_s$  is

proportional to  $a^2$ . According to these arguments, the two moduli may be expressed in terms of the porosity, grain size, and depth in the sediment as follows:

$$\gamma_p = \gamma_{po} \left[ \frac{(1 - N)u_g d}{(1 - N_o)u_{go}d_o} \right]^{1/3}, \quad (11)$$

and

$$\gamma_s = \gamma_{so} \left[ \frac{(1 - N)u_g d}{(1 - N_o)u_{go}d_o} \right]^{2/3}, \quad (12)$$

where the terms in brackets have been constructed to be dimensionless, with the factors  $\gamma_{po}$  and  $\gamma_{so}$  taking numerical values that are independent of the porosity, grain size, and depth in the sediment. By introducing the three reference parameters, porosity  $N_o$ , grain size  $u_{go}$ , and depth  $d_o$ , into the denominators of Eqs. (11) and (12), awkward dimensions are avoided when the terms in square brackets are raised to a fractional power. It should be clear that the values of these reference parameters may be chosen for convenience; they do not represent additional unknowns. To distinguish them from the compressional and shear moduli, the parameters  $\gamma_{po}$  and  $\gamma_{so}$ , respectively, will be referred to as compressional and shear coefficients. Obviously,  $\gamma_{po}$  and  $\gamma_{so}$  are the values of  $\gamma_p$  and  $\gamma_s$  when  $N = N_o$ ,  $u_g = u_{go}$ , and  $d = d_o$ .

In making the comparisons between the G-S theory and data, the values of the compressional and shear coefficients, as well as the strain-hardening index,  $n$ , are held fixed for all sediments, from coarse sands to the finest silts and clays. In principle, however,  $\gamma_{po}$ ,  $\gamma_{so}$ , and  $n$  could depend weakly on the elastic properties of the mineral grains and also on such factors as the micro-roughness of the areas of contact. Thus, in practice, the values of these three parameters could differ slightly from one sediment to another but, judging from the good quality of the match between theory and data, as demonstrated below, it would seem that such variations are very minor.

The functional dependence of the G-S dispersion relations on the macroscopic, geoacoustic parameters of a sediment are given explicitly and completely by the algebraic expressions in Eqs. (1) to (12). From a casual inspection, it is evident that the selection of geoacoustic parameters appearing in the G-S theory is quite different from that in Biot's theory.<sup>13,14</sup> According to Table 1.1 in Stoll,<sup>21</sup> the Biot theory involves the permeability, the viscosity of the pore fluid, the pore-size parameter, the structure factor, the (complex) shear modulus of the skeletal frame, and the (complex) bulk modulus of the skeletal frame, a total of eight parameters, all of which are absent from the G-S formulation of the dispersion relations. Instead, the G-S theory includes the three (real) parameters representing microscopic processes occurring at grain contacts,  $\gamma_{po}$ ,  $\gamma_{so}$ , and  $n$ . Through the compressional and shear moduli [Eqs. (11) and (12)], the G-S theory also includes the grain size and the depth in the sediment, neither of which appears explicitly in Biot's theory. The porosity, the bulk density, and the physical properties (densities and bulk moduli) of the individual constituents of the biphasic medium are common to both theories.

According to Eq. (5), the bulk density and the porosity are linearly related and hence are fully correlated. In fact,

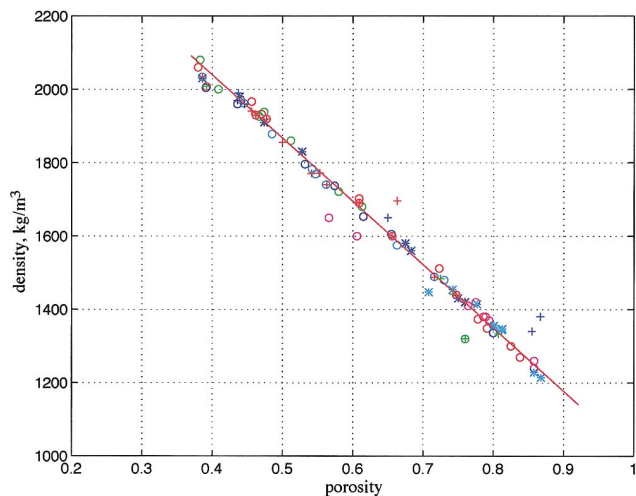


FIG. 1. Compilation of density versus porosity data, mostly from Hamilton. The red line is from Eq. (5) using the values of  $\rho_w$  and  $\rho_g$  listed in Table II. (See Table I for the key to the symbols in this and all subsequent figures.)

Richardson *et al.*<sup>10–12,22</sup> have used this relationship to compute the bulk density from laboratory measurements of the porosity. Hamilton,<sup>3,7,8</sup> on the other hand, measured the den-

sity directly from weight and volume, rather than computing it by substituting his independently measured porosity into Eq. (5). Hamilton's data may therefore be used as a test of Eq. (5).

Figure 1 shows Hamilton's published measurements of density and porosity for many types of marine sediment, ranging from very fine silts and clays to coarse sands. (Table I is the key to all the symbols, representing published data collected from the literature, which appear in Figs. 1 to 11). Also shown in Fig. 1 is a plot of the linear relationship between density and porosity in Eq. (5), evaluated with  $\rho_w = 1005 \text{ kg/m}^3$  and  $\rho_g = 2730 \text{ kg/m}^3$ . Most of the data points fall on or very close to the line, indicating that the correlation represented by Eq. (5) holds accurately in practice, making it unnecessary to examine the functional dependence of the wave properties on both the porosity and the bulk density. Porosity alone is considered below.

### III. EVALUATION OF $\gamma_{po}$ , $\gamma_{so}$ , AND $n$

As already discussed, in addition to the macroscopic variables (porosity, grain size, and depth in the sediment), the G-S dispersion relationships [Eqs. (1)–(4)] involve the three

TABLE I. Key to the data symbols in Figs. 1–11.

Symbol	Color	Source
○	Red	Hamilton (Ref. 5) (1972), Table 1
○	Green	Hamilton (Ref. 5) (1972), Table 2
○	Blue	Hamilton (Ref. 5) (1972), Table 3
○	Magenta	Hamilton (Ref. 3) (1970), Table 2
○	Cyan	Hamilton (Ref. 8) (1987), Tables 1 & 2
*	Blue	Hamilton (Ref. 3) (1970), Table 1
*	Cyan	Hamilton (Ref. 8) (1987), Tables 3 & 4
+	Red	Hamilton (Ref. 6) (1980), Table 1
+	Green	Hamilton <i>et al.</i> (Ref. 2) (1970), Table 2
+	Blue	Hamilton (Ref. 43) (1963), Table 1
⊕	Red	Hamilton (Ref. 44) (1956), Tables 1a & 1b
⊕	Green	Wood & Weston (Ref. 45) (1964),
○	Black	Buckingham & Richardson (Ref. 23) (2002), Tables 1a & 1b
+	Black	Richardson (Ref. 12) (2002), Fig. 1 & Richardson (Ref. 33) (2000) Fig. 2
⊕—⊕	Black	Richardson <i>et al.</i> (Ref. 25) (2001), Fig. 15
*—*	Black	Richardson (Ref. 10) (1991), Table 1 & Fig. 3
+	Cyan	Richardson (Ref. 46) (1986), Table 1
*	Magenta	Richardson <i>et al.</i> (Ref. 9) (1991), Tables 43.1 and 44.2
×	Red	Richardson & Briggs (Ref. 22) (1996), Figs. 3, 5, 6
×	Blue	Richardson (Ref. 11) (1997), Table 1, La Spezia & Adriatic Sea
×	Green	Richardson (Ref. 11) (1997), Table 1, Panama City & Boca Raton
×	Magenta	Richardson (Ref. 11) (1997), Table 1, Eckernfoerde Bay, Germany
×	Cyan	Richardson (Ref. 11) (1997), Table 1, Eel River & Orcas Bay
⊗	Green	Brunson & Johnson (Ref. 47) (1980), Table II
⊕	Magenta	Simpson <i>et al.</i> (Ref. 15) (2003), Fig. 6
⊗	Blue	Brunson (Ref. 48) (1991), Tables 1 & 2
*	Black	Richardson (Ref. 10) (1991), Table 1 & Fig. 3
+	Magenta	Richardson & Briggs (Ref. 49) (1993), Table 1
×	Black	McLeroy & DeLoach (Ref. 50) (1968), Table II
*	Red	McCann & McCann (Ref. 51) (1969), Table 3
*	Green	Richardson (Ref. 12) (2002), Fig. 3

TABLE II. Parameters appearing in the G-S dispersion relations.

Material parameter	Symbol	Value	Comments
Density of pore fluid (kg/m <sup>3</sup> )	$\rho_f$	1005	Evaluated from density versus porosity fit to data, Fig. 1
Bulk modulus of pore fluid (Pa)	$K_f$	$2.374 \times 10^9$	From Kaye & Laby (Ref. 52), p. 35
Density of grains (kg/m <sup>3</sup> )	$\rho_s$	2730	Evaluated from density porosity fit to data, Fig. 1
Bulk modulus of grains (Pa)	$K_t$	$3.6 \times 10^{10}$	From Richardson <i>et al.</i> (Ref. 53)
Compressional coefficient (Pa)	$\gamma_{po}$	$3.888 \times 10^8$	Evaluated from spot-frequency compressional and shear wave data
Shear coefficient (Pa)	$\gamma_{so}$	$4.588 \times 10^7$	Evaluated from spot-frequency compressional and shear wave data
Strain-hardening index	$n$	0.0851	Evaluated from spot-frequency compressional wave data
rms grain roughness ( $\mu\text{m}$ )	$\Delta$	1	Evaluated from porosity versus grain size distribution, Fig. 7(b)
Reference grain diameter ( $\mu\text{m}$ )	$u_o$	1000	Arbitrary choice
Reference depth in sediment (m)	$d_o$	0.3	Arbitrary choice
Reference porosity	$N_o$	0.377	Arbitrary choice
Porosity	$N$	Variable	
Mean grain diameter ( $\mu\text{m}$ )	$u_g$	Variable	
Depth in sediment (m)	$d$	Variable	

unknown constants,  $\gamma_{po}$ ,  $\gamma_{so}$ , and  $n$ , which characterize the microscopic interactions occurring at grain boundaries during the passage of compressional and shear waves. At present, no theory exists from which these constants could be computed, so instead they are evaluated here from spot-frequency measurements of three wave properties: the compressional speed, the compressional attenuation, and the shear speed.

The two compressional-wave observations are taken from Table 1a in Buckingham and Richardson<sup>23</sup> for the SAX99 medium-sand sediment [ $u_g = 414.7 \mu\text{m}$  ( $\phi = 1.27$ ),  $N = 0.377$ ]: at depth  $d = 0.3$  m and a frequency of 100 kHz, the measured sound speed (cf) and attenuation ( $\alpha$ f) are 1787 m/s and 30.93 dB/m, respectively. The shear-speed measurement, taken from Fig. 1 in Richardson,<sup>12</sup> is for a well-sorted, fine-sand sediment [ $u_g = 238.16 \mu\text{m}$  ( $\phi = 2.07$ ),  $N = 0.358$ ] at a North Sea site designated C1: at depth  $d = 0.28$  m and a frequency of 1 kHz, the (average) shear speed is 131.4 m/s.

When the measurements cited above are substituted into the compressional and shear dispersion relations [Eqs. (1)–(4)], some elementary algebra yields the values of  $\gamma_{po}$ ,  $\gamma_{so}$ , and  $n$  listed in Table II. In the following comparisons of the G-S theory with numerous data sets, these values are held fixed for *all* sediments. Under this constraint, it is of some interest to examine how well the G-S dispersion relationships represent the wave properties in sediments ranging from coarse sands to very fine clays. This is achieved by considering the dependencies of the wave speeds and attenuations on porosity and grain size. The depth dependence of the wave properties is also compared with data from various types of sediment. As will become evident, the fixed values of  $\gamma_{po}$ ,  $\gamma_{so}$ , and  $n$  cited in Table II lead to theoretical wave-property dependencies on porosity, grain size, and depth that align with essentially all the data. Before discussing the physical properties, however, the theoretical dependencies of the wave speeds and attenuations on frequency are compared with observations.

As mentioned earlier, most of the data used in the following comparative discussions are from *in situ* measurements made in siliclastic (quartz sand) sediments. Carbonate sediments are excluded, since they differ from siliclastic materials in several ways,<sup>24</sup> including having open, hollow grains, which, with all else equal, gives rise to higher porosities. Hamilton and Bachman<sup>7</sup> found that “hollow tests (shells) of Foraminifera act as solid particles in transmitting sound,” implying that the intraparticle porosity had little if any effect on the wave properties. A preliminary comparison between wave data from carbonate sediments and the G-S theory, evaluated using the interparticle (rather than total) porosity, appears to support Hamilton and Bachman’s conclusion but requires more detailed examination before being discussed further.

## IV. FREQUENCY DEPENDENCE

### A. Compressional wave

Figure 2 shows *in situ* measurements of the frequency dependence, from 25 to 100 kHz, of the compressional wave speed and attenuation at the SAX99, medium-sand experiment site off Fort Walton Beach in the northern Gulf of Mexico.<sup>25</sup> The smooth curves, representing the G-S theory, were evaluated from Eqs. (1) and (2). These theoretical curves pass precisely through the higher of each pair of data points at 100 kHz as expected, since both data points were used in evaluating the compressional and shear coefficients  $\gamma_{po}$ ,  $\gamma_{so}$  as well as the strain-hardening index,  $n$ .

The sound-speed data from the SAX99 site [Fig. 2(a)] exhibit weak logarithmic dispersion at a level of approximately 1% per decade of frequency. A similar logarithmic gradient is predicted by the G-S theory. Although there is some scatter in the data (of the order of  $\pm 10$  m/s), it is clear that the measured sound speeds cluster around the theoretical line. The observed SAX99 dispersion is consistent with recently reported *in situ* measurements by Simpson *et al.*,<sup>15</sup>

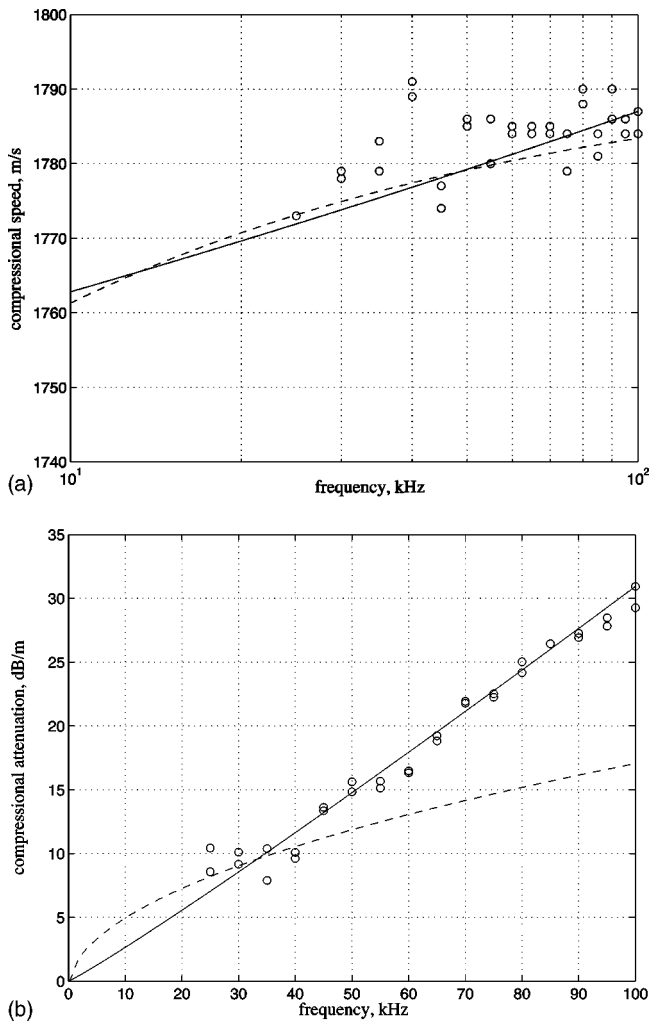


FIG. 2. Measured frequency dependence of the compressional (a) speed (semilogarithmic axes) and (b) attenuation (linear axes) for the medium-sand SAX99 site. The smooth, solid curves represent the predictions of the G-S theory, computed from Eqs. (1) and (2) using the reported values (Ref. 25) of the porosity, grain size, and depth [ $N=0.377$ ,  $u_g=414.7 \mu\text{m}$  ( $\phi=1.27$ ),  $d=0.3 \text{ m}$ ]. The dashed curves are from William's EDF approximation (Ref. 29) to the Biot theory, with  $\kappa=2.5 \cdot 10^{-11} \text{ m}^2$  and  $A=1.35$ .

which were made in a medium-sand sediment at St. Andrews Bay, Florida. Over the frequency band from 3 to 80 kHz, they also observed logarithmic dispersion in the region of 1% per decade. Such a weak gradient is quite difficult to detect *in situ*, and earlier investigators not uncommonly failed to observe any variation of sound speed with frequency. Hamilton,<sup>4</sup> for example, reported that "there is negligible dependence or no dependence of velocity on frequency," on the basis of which he developed his empirical elastic model of wave propagation in sediments.

Visual inspection of the data in Fig. 2(b) reveals that, between 25 and 100 kHz, the compressional attenuation from the SAX99 site scales almost exactly as the first power of frequency. In fact, a straight line may be drawn through the data points which, when extrapolated, passes precisely through the origin. However, it has long been known that a pure linear scaling of attenuation with frequency is unphysical in that it violates causality.<sup>26–28</sup> But, no such difficulty arises with the G-S theory, which yields an attenuation that is

almost but not quite linear in frequency, as exemplified in Fig. 2(b). This near-linear curve, which rises marginally faster than the first power of frequency, passes through the origin and accurately through the data points.

The question of whether the attenuation in marine sediments varies (nearly) linearly with frequency has been a controversial issue for many years. Hamilton<sup>8</sup> consistently maintained, on the basis of extensive measurements made by himself and others, that the attenuation exhibits a linear scaling with frequency. Stoll,<sup>21</sup> on the other hand, has long argued on the basis of the Biot theory<sup>13,14</sup> that the attenuation deviates significantly from a first-power dependence on frequency, varying as the square root of frequency over the bandwidth of the data shown in Fig. 2(b).

Biot's dispersion curves, evaluated from Williams's<sup>29</sup> "effective density fluid" (EDF) approximation to Biot's full theory, are included as the dashed lines in Fig. 2. To compute the EDF sound speed and attenuation curves, the values of two physical parameters peculiar to the Biot theory, the permeability,  $\kappa=2.5 \times 10^{-11} \text{ m}^2$  and tortuosity  $A=1.35$ , were taken from Table 1 in Williams *et al.*,<sup>30</sup> which lists properties of the SAX99 sediment. In Fig. 2(a), it can be seen that the EDF sound speed shows weak dispersion, aligning reasonably with both the data and the G-S curve, although at lower frequencies than those shown the two theoretical predictions diverge. The EDF attenuation in Fig. 2(b), however, fails to match the data over most of the frequency range. Whereas the attenuation data scale essentially linearly with frequency, the EDF attenuation curve exhibits the classic, high-frequency  $f^{1/2}$  dependence of a viscous fluid.

Since viscous dissipation of the pore fluid is the only loss mechanism in the Biot theory,<sup>13,14</sup> it is not surprising that the frequency dependence of the Biot attenuation is exactly the same as that of a true viscous fluid.<sup>31</sup> Although the details of Biot's attenuation curve may vary with material parameters such as permeability and tortuosity, the functional form is always the same: at low frequencies the attenuation scales as the square of frequency, transitioning at about 1 kHz (depending on permeability and viscosity) to a square-root scaling with frequency. The discrepancy, illustrated in Fig. 2(b), between such behavior and the near-linear scaling of the attenuation data with frequency is a strong indicator that the viscous dissipation mechanism of the Biot theory may be insignificant in marine sediments.

Evidence to support such a conclusion is found not only in the SAX99 attenuation data. From 3 to 80 kHz, Simpson *et al.*<sup>15</sup> have observed a (near) linear dependence of attenuation on frequency (their Fig. 6) in a medium-sand sediment in St. Andrews Bay, Florida; and earlier laboratory experiments in fine sand by Simpson *et al.*<sup>32</sup> returned a similar (near) linear scaling of the attenuation with frequency between 4 and 100 kHz (their Fig. 7). As illustrated in Fig. 2(b), Biot's theory cannot account for a linear scaling of attenuation with frequency; but, such behavior is consistent with Hamilton's observations and also the predictions of the G-S theory.

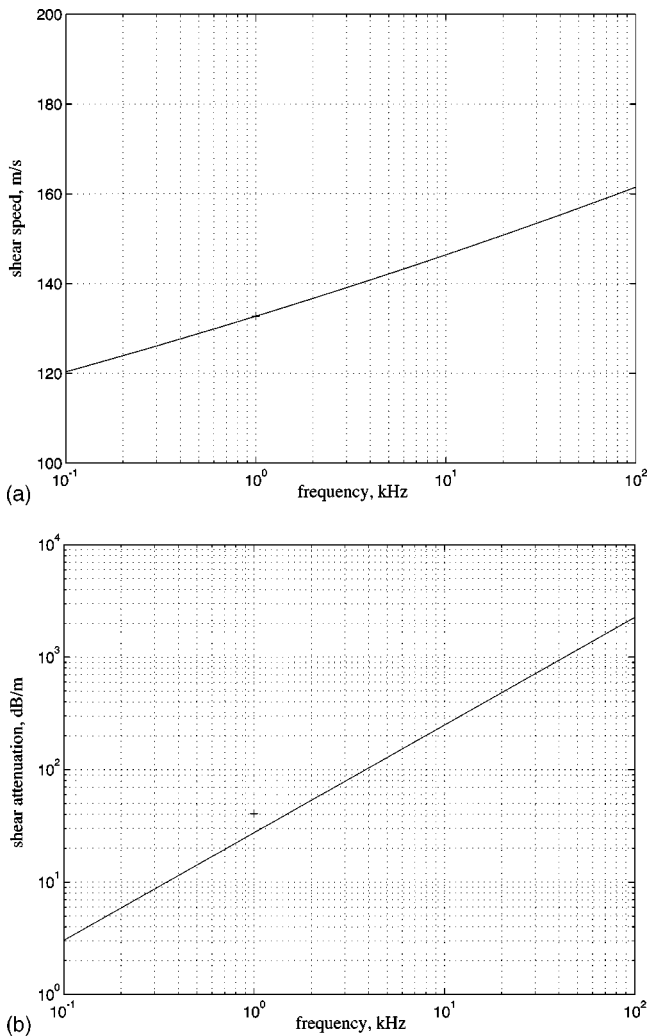


FIG. 3. Shear-wave (a) speed and (b) attenuation versus frequency from Richardson's North Sea site C1, well-sorted fine sand. The solid lines were evaluated from Eqs. (3) and (4) using the reported values (Ref. 33) of the porosity, grain size, and depth for the site [ $N=0.358$ ,  $u_g=238.2 \mu\text{m}$  ( $\phi=2.07$ ),  $d=0.28 \text{ m}$ ].

## B. Shear wave

*In situ* measurements of shear-wave properties as functions of frequency are rarer than those of compressional waves. In fact, no published, *in situ* measurements of shear-wave dispersion and attenuation over extended frequency ranges are known to the author.

The shear-wave speed and attenuation predicted from the G-S dispersion relations in Eqs. (3) and (4) are shown in Fig. 3. The curves were computed using values of the porosity, grain size, and depth in the sediment appropriate to Richardson's<sup>12</sup> North Sea site C1. The theoretical curve for the shear speed in Fig. 3(a) shows dispersion at a level of approximately 10% per decade of frequency, which is stronger than the dispersion in the compressional wave by a factor of 10 or so. It is evident from the uniform gradient of the curve in Fig. 3(a) that the predicted shear dispersion is logarithmic as expected, since  $c_s$  scales as  $f^{n/2}$  in Eq. (3). The lone shear-speed datum in Fig. 3(a) falls precisely on the theoretical curve, since it was used in the evaluation of the compressional and shear coefficients,  $\gamma_{po}$  and  $\gamma_{so}$ . The pre-

dicted shear attenuation in Fig. 3(b) can be seen to exhibit a (near) linear dependence on frequency, varying as  $f^{1-n/2}$ . Note that the theoretical curve passes below but close to the sole reported data point<sup>33</sup> taken at a frequency of 1 kHz. This agreement provides a mild test of the G-S theory, since the shear attenuation was not used in computing  $\gamma_{po}$ ,  $\gamma_{so}$ , or  $n$ . A single data point, of course, provides no information on the slope of the shear attenuation versus frequency curve, which is unfortunate because the gradient (as in the case of the compressional attenuation) provides an important test of theoretical models of waves in sediments. *In situ* measurements of shear dispersion and attenuation over extended frequency ranges are challenging but would be extremely useful for future validation of theoretical predictions.

## V. DEPTH DEPENDENCE

### A. Compressional wave

Published *in situ* data on the depth dependence of the sound speed and attenuation immediately beneath the seawater-sediment interface are scarce. Hamilton<sup>34,35</sup> discussed the variation of the sound speed with depth, but focused mainly on significantly greater depths than the meter or two of interest here. However, he did briefly consider the variation of the sound speed in the first 20 m of sand sediments,<sup>34</sup> for which he developed the following empirical power-law relationship, based on a curve fit to laboratory data:

$$c_{pH} = 1806d^{0.015}. \quad (13)$$

According to this expression, the sound speed is zero at the seawater-sediment interface and increases rapidly in the first meter or so, after which the rate of change slows significantly. No allowance for any variation of the sound speed with porosity is made in Eq. (13).

Hamilton<sup>36</sup> also considered the attenuation of sound as a function of depth. Based on laboratory measurements<sup>37,38</sup> of the variation of attenuation with confining pressure, he proposed an empirical inverse power-law relationship for the attenuation versus depth in sand

$$\alpha_{pH} = 0.45d^{-1/6}, \quad (14)$$

where the units of  $\alpha_{pH}$  are dB/m/kHz. Again, porosity is absent from this empirical representation. According to Eq. (14), the attenuation is infinite at the seawater-sediment interface but decreases very rapidly in the first few centimeters. It seems from curve B in Hamilton's<sup>36</sup> Fig. 3 that he considered Eq. (14) to be valid down to a depth of 150 m. Within the first few meters of the interface, however, his data are too poorly resolved in depth to say whether they support the strong negative gradient exhibited by Eq. (14).

Since Hamilton's<sup>8</sup> final review of the acoustic properties of sediments was published in 1987, few *in situ* measurements of near-interface sound-speed and sound-attenuation profiles in sand sediments have appeared in the literature. Acoustic profiles from cores, however, are available, some of the most recent being from Richardson *et al.*<sup>25</sup> for the SAX99 site. They measured sound speed and attenuation as functions of depth in a large number of cores at a frequency

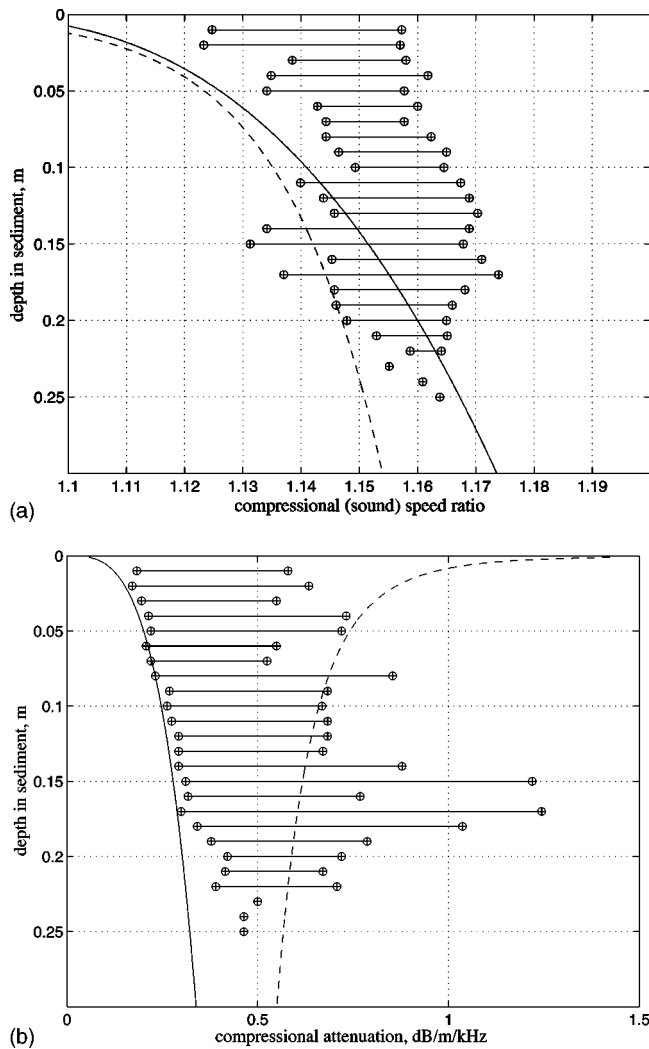


FIG. 4. Sound-speed (a) ratio and (b) attenuation versus depth for the medium-sand SAX99 site. The measurements were made on diver-collected cores at 400 kHz and each horizontal line represents the spread of the data at a given depth. The smooth solid lines, representing the G-S theory, were evaluated from Eqs. (1) and (2) using the reported values (Ref. 25) of the porosity, grain size, and measurement frequency [ $N=0.377$ ,  $u_g=414.7 \mu\text{m}$  ( $\phi=1.27$ ),  $f=400 \text{ kHz}$ ]. The dashed lines, depicting Hamilton's empirical profiles, were evaluated from Eqs. (13) and (14).

of 400 kHz. The results are shown in Fig. 4, along with the G-S theory (smooth solid lines), evaluated taking the porosity as independent of depth.<sup>39</sup> Hamilton's empirical expressions are also included (dashed lines) for comparison. It should be noted that the G-S attenuation was computed for a frequency of 400 kHz and then divided by 400, to obtain the attenuation profile shown in Fig. 4(b), having units of dB/m/kHz. This procedure is consistent with that applied to the data. For the purpose of making the comparison between theory and data in Fig. 4(b), it would have been inappropriate to compute the attenuation directly for a frequency of 1 kHz, since this would have underestimated the theoretical result (relative to the data) due to the slight nonlinear dependence of the G-S attenuation on frequency [Fig. 2(b)].

At each depth increment, the sound speed and attenuation data show some spread, as indicated by the horizontal bars in Fig. 4. Note, however, that the variations in the sound speed are less than  $\pm 2\%$ , whereas those in the attenuation

are of the order of  $\pm 40\%$ . As discussed below, this relatively high variability in the attenuation data may be attributable to various factors including scattering from inclusions such as shell fragments in the sediment as well as random coupling losses, which are expected whenever a sensor is inserted into a granular sedimentary medium.

Below a depth of 10 cm, the G-S theory yields a sound-speed profile that falls within the limits of the data in Fig. 4(a). At shallower depths, where the gradient in the sound speed is very high, the G-S theory falls a little below the lower limits of the data. This small discrepancy between the theory and the data may be due to the difficulty of measuring the sound speed near the interface, where the gradient of the upward-refracting profile is particularly steep: diving waves may reach the receiver first, giving rise to an overestimate of the sound speed. Note that the trends of the G-S sound-speed profile and Hamilton's empirical relationship are similar, with both showing a rapid increase within a few centimeters of the interface. In the case of the G-S profile, this high, near-interface gradient is an effect of the overburden pressure, which gives rise to a high rate of increase of the compressional coefficient [Eq. (11)] immediately below the boundary. At the boundary itself ( $d=0$ ), the G-S profile takes Wood's value,  $c_o$ , whereas Hamilton's expression goes to zero.

Turning to the attenuation profiles in Fig. 4(b), it appears that the negative gradient of Hamilton's empirical curve is not consistent with the data (even allowing for the fact that the data show considerable spread). On the other hand, the G-S attenuation profile accurately tracks the lower-limiting values of the measured attenuation. As will become apparent, the G-S theory systematically delineates the lower limits of all the (compressional and shear) attenuation data sets examined in this paper, that is, the G-S theory traces the lower bound to the envelope of the measured attenuation values.

A plausible interpretation of this observation is that the G-S theory predicts the *intrinsic* attenuation due to intergranular interactions, which convert acoustic energy into heat, whereas the measurements represent the *effective* attenuation, that is, the total attenuation experienced by a sound or shear wave in propagating through the granular material. Thus, in addition to the intrinsic attenuation, the effective attenuation includes all other losses, notably those due to scattering from inhomogeneities such as shell fragments in the medium. Naturally, since shells and other scatterers are likely to be distributed randomly throughout the sediment, the effective attenuation is expected to be highly variable, but with a lower limiting value equal to the intrinsic attenuation. According to this argument, the G-S theory is expected to coincide with the lower bound of the data, as indeed it does in Fig. 4(b).

## B. Shear wave

Figure 5(a) shows Richardson's<sup>12</sup> *in situ* measurements of the shear speed versus depth at 1 kHz in well-sorted fine sand at the North Sea C1 site. At each depth, the data point in Fig. 5(a) represents the mean of the several measured values reported by Richardson.<sup>12</sup> The data display a distinct positive gradient, with the shear speed approximately doubling be-

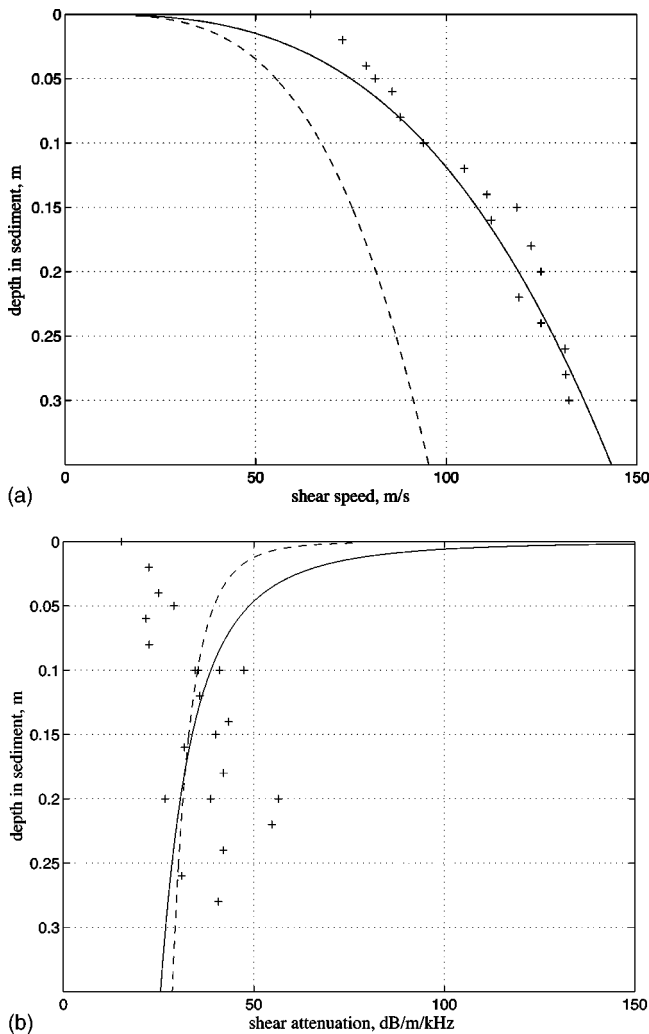


FIG. 5. Shear-wave (a) speed and (b) attenuation versus depth for the well-sorted fine sand at North Sea site C1. The smooth solid lines, representing the G-S theory, were evaluated from Eqs. (3) and (4) along with Eq. (12) using the reported values (Ref. 33) of the porosity, grain size, and measurement frequency [ $N=0.358$ ,  $u_g=238.2 \mu\text{m}$  ( $\phi=2.07$ ),  $f=1 \text{ kHz}$ ]. The dashed lines are Hamilton's empirical profiles, as given by Eqs. (15) and (16).

tween depths of 5 and 30 cm. Similar behavior is predicted by the G-S theory [Eqs. (3) and (12)], as shown by the smooth solid line in Fig. 5(a), which increases as the cube root of depth in the sediment. In evaluating the G-S line in Fig. 5(a), the porosity was taken to be independent of depth, consistent with the porosity profiles measured on cores<sup>25</sup> and *in situ*<sup>39</sup> during the SAX99 experiment. It is clear that the theoretical curve in Fig. 5(a) closely matches the experimentally determined shear-speed profile.

The cube root of depth power law from the G-S theory is similar in form to an empirical shear-speed profile for sand sediments proposed by Hamilton<sup>8</sup>

$$c_{sH} = 128d^{0.28}. \quad (15)$$

This expression is plotted in Fig. 5(a) as the dashed line. In fact, Hamilton<sup>8</sup> discussed several empirical expressions having the form of Eq. (15) but with slightly different exponents, ranging from 0.25 to 0.312. Over the limited depth range of Richardson's data,<sup>12</sup> these exponents are almost indistin-

guishable, not only from one another but also from the G-S exponent of 1/3. However, Hamilton's (fixed) coefficient of 128 in Eq. (15) significantly underestimates Richardson's data in Fig. 5(a), by approximately 30% at a depth of 30 cm. It should be noted that, according to Eq. (12), the corresponding coefficient in the G-S theory is a function of porosity and grain size, and thus may differ from one sediment to another. Equation (15) obviously does not accommodate such behavior.

The shear attenuation measured by Richardson<sup>33</sup> at the North Sea C1 site is shown in Fig. 5(b). Included in the figure is the G-S theoretical prediction evaluated from Eqs. (4) and (12), again taking the porosity as independent of depth.<sup>25,39</sup> It is evident from these equations that the predicted attenuation scales as the reciprocal of the cube root of depth and that the coefficient of proportionality is a function of porosity and grain size. Below a depth of 10 cm, the G-S theory follows the lower bound of the attenuation data, which is consistent with the earlier argument that the G-S curve depicts intrinsic attenuation, as opposed to the effective attenuation represented by the data. At shallower depths, the G-S theory overestimates the measured attenuation, but Richardson<sup>33</sup> has suggested that these near-interface data points may in fact be too low as a result of ducting (diving waves) produced by the steep shear-speed gradient within the upper few centimeters of the sediment.

Hamilton<sup>8</sup> has proposed the following empirical expression for the shear attenuation profile:

$$\alpha_{sH} = 24d^{-1/6}, \quad (16)$$

which is shown as the dashed line in Fig. 5(b). Note that Hamilton's inverse-fractional-power-law scalings for the compressional attenuation [Eq. (14)] and shear attenuation [Eq. (16)] are exactly the same, both having an exponent of  $-1/6$ . Like the G-S shear attenuation profile, Eq. (16) shows a steep negative gradient immediately below the interface, whereas the gradient of Richardson's data is weakly positive. As mentioned above, this discrepancy may be the result of ducting just below the interface.

Figure 6 shows the shear-speed profiles of three finer-grained sediments, measured *in situ* by Richardson *et al.*<sup>10</sup> at Boa Dragaggio (fine sands and silt clays), Viareggio (silt clay), and Portovenere (silt and clay). (No shear-attenuation data were reported for these sites.) In all three cases, the shear speed is significantly less than that at the fine-sand, North Sea C1 site shown in Fig. 5(a). Notice the subtle differences between the Boa Dragaggio, Viareggio, and Portovenere profiles, and the fact that all three profiles are accurately reproduced by the G-S theory, evaluated from Eqs. (3) and (12) using the reported porosities and grain sizes.

The difference between the observed shear-speed profiles at Boa Dragaggio and Viareggio [Figs. 6(a) and 6(b)] is particularly interesting, since the reported porosities of these two sediments are almost the same, at 0.57 and 0.58, respectively. It follows that the difference in the shear speeds at the two sites, amounting to about 10 m/s at a depth of 2 m, must be due to the difference between the mean grain sizes. Boa Dragaggio is the coarser of the two sediments, with a reported mean grain diameter<sup>10</sup> of  $3.4 \mu\text{m}$  ( $\phi=8.2$ ), compared

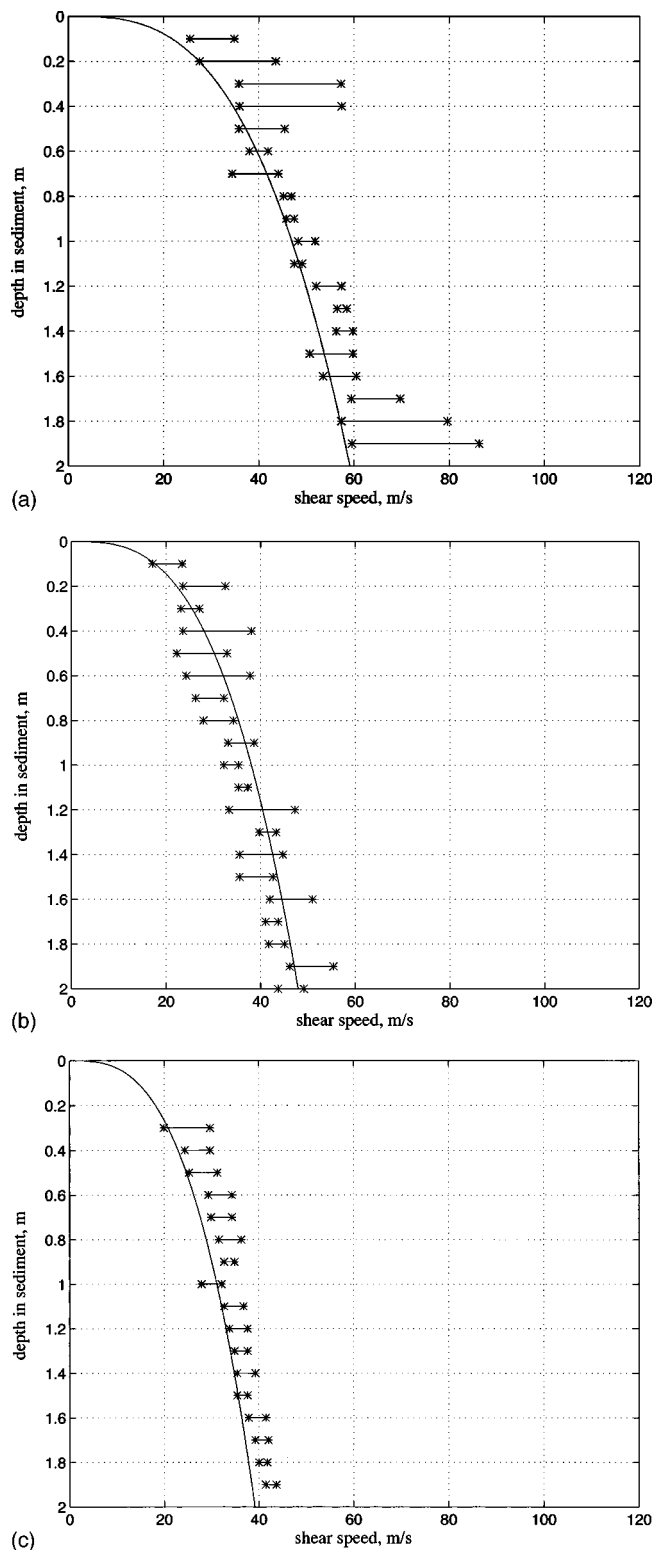


FIG. 6. Shear-speed profiles from (a) Boa Dragaggio [ $N=0.57$ ,  $u_g = 3.4$  micron ( $\phi=8.2$ ),  $f=1$  kHz]; (b) Viareggio [ $N=0.58$ ,  $u_g = 1.82$  micron ( $\phi=9.1$ ),  $f=1$  kHz]; and (c) Portovenere [ $N=0.63$ ,  $u_g = 1.05$  micron ( $\phi=9.9$ ),  $f=300$  Hz]. The smooth curves, representing the G-S theory, were evaluated from Eqs. (3) along with Eq. (12) using the reported values (Ref. 10) of the porosity, grain size, and measurement frequency for each of the sites, as listed here in square brackets.

with  $1.82 \mu\text{m}$  ( $\phi=9.1$ ) at Viareggio. In the G-S theory, the grain size affects the shear speed only through the shear modulus,  $\gamma_s$ , given by Eq. (12). According to this expression, the shear modulus for Boa Dragaggio is greater than that for Viareggio by a factor of 1.5. This is sufficient to give rise to slightly dissimilar theoretical shear-speed profiles for the two sites, in excellent agreement with the data, as shown in Figs. 6(a) and 6(b).

At the Portovenere site [Fig. 6(c)], the porosity is marginally higher and the grain size a little lower than at Boa Dragaggio and Viareggio. The enhanced porosity affects the bulk density,  $\rho_o$  in Eq. (5), and also the shear modulus,  $\gamma_s$  in Eq. (12), while the smaller grain size influences only  $\gamma_s$ . The net effect, as predicted by Eq. (3), is a slightly slower shear-speed profile than that at either of the other two sites. Again, it can be seen that the theoretical curve and the data are in very good agreement.

## VI. RELATIONSHIPS BETWEEN PHYSICAL PROPERTIES

Although the porosity, grain size, and bulk density appear independently in the G-S dispersion expressions, these quantities are not themselves independent: finer-grain sediments tend to have lower densities and higher porosities than coarser materials. In order to evaluate the G-S dispersion relations as a function of any one of the three physical properties, porosity, grain size, and density, it is necessary first to establish the relationships that exist between them.

Of these inter-relationships, that between bulk density and porosity is well known and has already been introduced as the linear combination of the two constituent densities in Eq. (5). This expression accurately matches the data, as exemplified in Fig. 1. It follows that, provided the densities of the fluid and mineral phases are known, the bulk density can be determined directly from measurements of the porosity and vice versa.

The functional dependence of porosity on grain size is more difficult to treat, not least because porosity is not uniquely determined by grain size: sediments with identical porosities may exhibit mean grain sizes that differ from one another, as exemplified by the sediments investigated by Richardson *et al.*<sup>10</sup> at Boa Dragaggio and Viareggio [see Figs. 6(a) and (b)]. Interestingly, Hamilton's data on porosity versus grain size show a significantly smaller scatter than the corresponding data collected from numerous sites by Richardson, a difference that becomes clear on comparing Figs. 7(a) and 7(b). However, a trend common to both data sets is that finer-grain sediments tend to exhibit higher porosities.

Any variation of the porosity with grain size represents a departure from the way smooth, uniform spheres pack together. Hamilton<sup>8</sup> has attributed the observed variation of porosity with grain size, illustrated in Fig. 7, to several factors including nonuniformity in the size and the shape of the grains.

Amongst unconsolidated marine sediments, the lowest porosities are found in the coarse sands, almost always taking values close to 0.37. As it happens, 0.37 is also the porosity of a random "close" packing of smooth, uniform

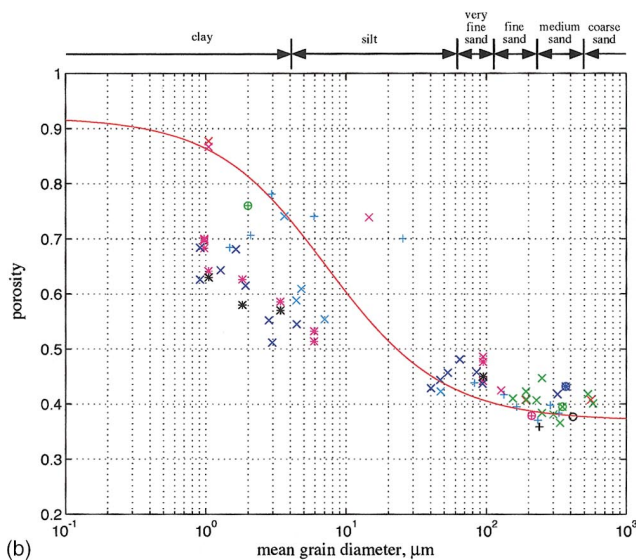
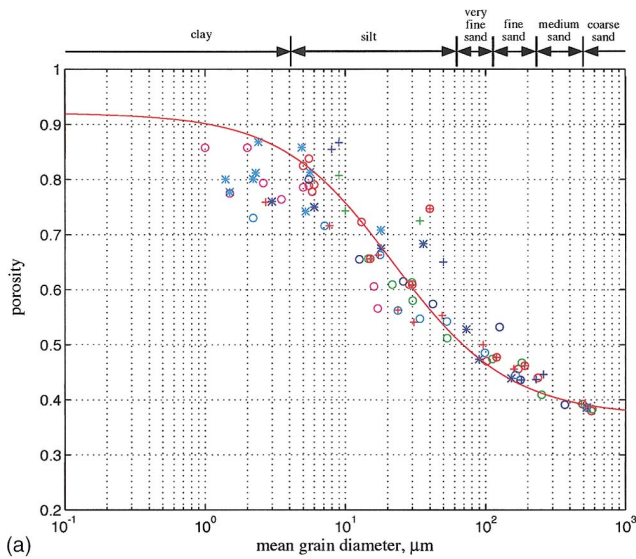


FIG. 7. Porosity versus grain size. (a) Comparison of Hamilton's data with Eq. (17), evaluated taking  $\Delta=3 \mu\text{m}$  (red curve). (b) Comparison of Richardson's data with Eq. (17), taking  $\Delta=1 \mu\text{m}$  (red curve).

spheres,<sup>40,41</sup> which suggests that, in the coarser sediments, grain shape (or roughness) effects represent a negligible departure from sphericity, and thus the packing is much like a random packing of smooth spheres. In the finer-grained sediments, on the other hand, surface roughness may be comparable with or much greater than the mean grain diameter, in which case close contact between adjacent grains is prevented, thus allowing pore water to percolate between grains, which results in an increase in the porosity. Grain "shape" and "roughness" in this context cover a multitude of non-spherical conditions, encompassing smooth, potato-like grains, high-aspect-ratio platelets, and very spiky, hedgehog-like particles.

Based on these ideas (i.e., a random packing of rough spheres), Buckingham<sup>42</sup> developed the following relationship between porosity and grain size:

$$N = 1 - P_s \left\{ \frac{u_g + 2\Delta}{u_g + 4\Delta} \right\}^3, \quad (17)$$

where  $P_s=0.63$  is the packing factor of a random arrangement of smooth spheres and  $\Delta$  is the rms roughness measured about the mean (equivalent volume sphere) surface of the grains. The inverse of Eq. (17) gives the grain size as a function of the porosity

$$u_g = \frac{2\Delta(2B-1)}{1-B}, \quad (18)$$

where

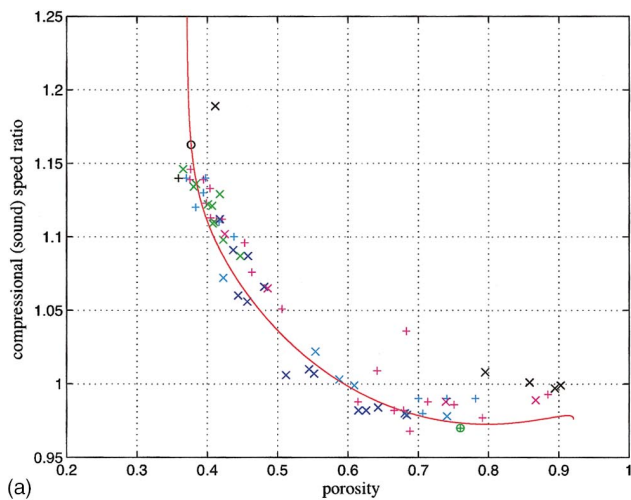
$$B = \left\{ \frac{1-N}{1-N_{\min}} \right\}^{1/3}. \quad (19)$$

According to Eq. (17), when the grain size is very much greater than the rms roughness, the porosity approaches its minimum value,  $N_{\min}=1-P_s=0.37$ , appropriate to the coarse-sand regime of Fig. 7. At the other extreme, when the roughness is very much greater than the grain diameter, as with the high-aspect-ratio clay and silt particles, the porosity takes its maximum value,  $N_{\max}=1-(P_s/8)=0.92$ , which conforms with the fine-grain, high-porosity data in Fig. 7.

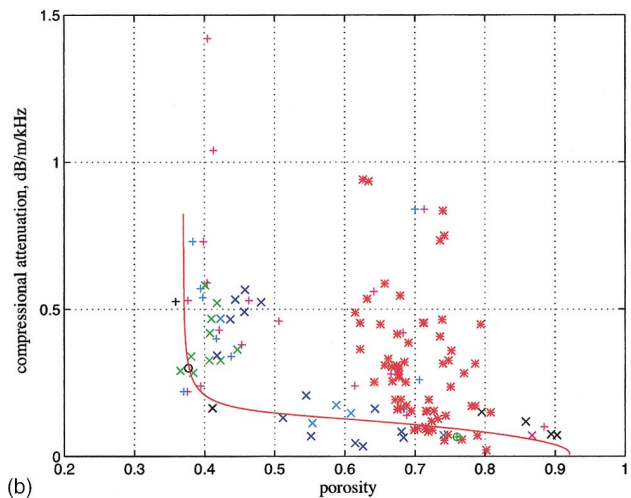
It is clear from the presence of  $\Delta$ , the rms roughness parameter, in Eq. (17) that sediments of nominally the same mean grain size may exhibit different porosities. A sharp sand having very rough grains (high  $\Delta$ ) may be considerably more porous than an otherwise similar smooth-grained sand (low  $\Delta$ ). Although the rms roughness of the grains is not a parameter that is normally reported, the value of  $\Delta=3 \mu\text{m}$  yields a relationship between porosity and grain size from Eq. (17) that follows the average trend of Hamilton's data in Fig. 7(a), whereas a somewhat lower value of  $\Delta=1 \mu\text{m}$  is more appropriate to the average of Richardson's data, as illustrated in Fig. 7(b).

It is not clear why Hamilton's and Richardson's data sets in Figs. 7(a) and 7(b), respectively, should differ so markedly. The differences appear not only in the average trends but also in the scatter of the data about the mean porosity, especially for the finer-grained materials, a spread which is noticeably greater in Richardson's data. Perhaps the reason for the disparities between the two data sets is nothing more than coincidence in that the majority of the sediments examined by Richardson just happened to have smoother grains, and hence lower porosities, than those analyzed by Hamilton.

In order to make comparisons between the theoretical and measured wave properties as functions of the porosity and the grain size, an "optimum" value of  $\Delta$  must be selected for substitution into Eq. (17). Since most of the data in the following comparisons stem from Richardson's measurements, the value of  $\Delta=1 \mu\text{m}$  is adopted for the rms roughness parameter, consistent with the comparison between data and theory in Fig. 7(b). With a fixed value of  $\Delta$  in Eq. (17), the theoretical predictions of the wave properties from the G-S dispersion relations are, of course, single valued in the porosity and in the grain size, but the resultant curves are useful for comparison with the average trends of the multi-valued experimental data.



(a)



(b)

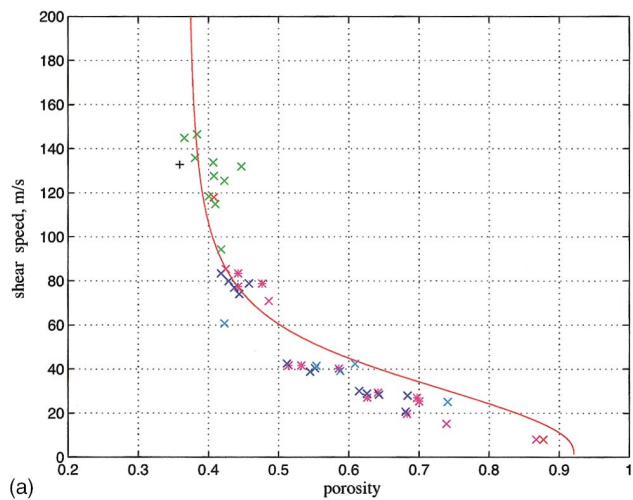
FIG. 8. (a) Sound-speed ratio versus porosity and (b) sound attenuation versus porosity. The red curves were evaluated from the G-S theory [Eq. (1)] with  $f=38$  kHz and  $d=0.3$  m, and  $\Delta=1 \mu\text{m}$  in Eq. (17). To obtain the attenuation in dB/m/kHz, for comparison with the data, the value computed at 38 kHz was divided by 38.

## VII. POROSITY DEPENDENCE

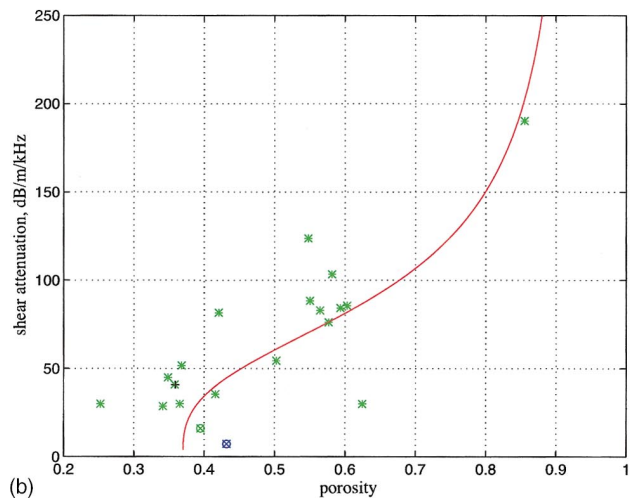
### A. Compressional wave

The ratio of the sound speed in the sediment divided by that in the water column is much less sensitive to temperature variations amongst sediments than the sound speed itself. Figure 8(a) shows a plot of the sound-speed ratio versus porosity computed from the G-S theory [Eq. (1)], along with data from a large number of sediments. The abundance of data points in Fig. 8(a) reveals a clear trend over the porosity range from  $N \approx 0.37$  to  $N \approx 0.92$ , covering coarse sands to clays. Throughout this range, the theoretical curve accurately follows the trend of the data.

An interesting feature of both the data and the theoretical curve in Fig. 8(a) is the extremely steep gradient of the sound speed at porosities corresponding to the coarser sands ( $0.37 < N < 0.4$ ). As the porosity rises marginally above its lower limit of 0.37, the sound speed plummets, eventually passing through a broad minimum around  $N \approx 0.8$ . In view of the sensitivity to the porosity in the coarser materials, it is essential to have a high-precision measure of  $N$  available if



(a)



(b)

FIG. 9. (a) Shear-wave speed versus porosity and (b) shear-wave attenuation versus porosity. The red curves were evaluated from the G-S theory [Eqs. (3) and (4)] with  $f=1$  kHz and  $d=0.3$  m, and  $\Delta=1 \mu\text{m}$  in Eq. (17). [Note: The shear wave data reported in several of Hamilton's papers were mostly determined indirectly from measurements of interface waves. As they appear to be distinctly different in character from more recent direct measurements of shear wave properties, his data are not included in these plots.]

the sound speed for a sand sediment is to be predicted accurately from the G-S theory.

The compressional attenuation as a function of porosity is shown in Fig. 8(b), where the smooth curve was computed by evaluating the G-S attenuation [Eq. (2)] for a frequency of 38 kHz (i.e., the frequency at which most of the data were collected) and dividing the result by 38 to obtain the predicted attenuation in dB/m/kHz. It is evident that the scatter is much higher in the attenuation data [Fig. 8(b)] than in the sound-speed data [Fig. 8(a)]. As with the depth profiles of attenuation in Fig. 4(b) (compressional) and Fig. 5(b) (shear), the G-S theoretical curve tracks the lower bound of the widely spread attenuation data in Fig. 8(b) (if allowance is made for relatively large measurement errors in the lowest attenuations). Such behavior is consistent with the fact that the theory predicts the intrinsic attenuation, due to the irreversible conversion of wave energy into heat, whereas the measurements represent the randomly distributed effective attenuation. As discussed earlier, in addition to the intrinsic attenuation, the effective attenuation includes all other types

of loss, due for instance to scattering from inhomogeneities such as shell fragments in the medium.

Like the sound speed, the theoretical intrinsic attenuation decays extremely rapidly as the porosity rises incrementally above the minimum value of 0.37, with a similar rapid decay exhibited by the data. It follows that, in order to predict accurately the intrinsic attenuation in a sand sediment, a high-precision estimate of the porosity is required.

## B. Shear wave

Figure 9(a) shows the speed of the shear wave as a function of porosity, with the smooth curve representing the G-S theory [Eq. (3)]. The clear downward trend in the data is reproduced well by the theoretical curve. The finer, high-porosity sediments exhibit the slowest shear speeds, with values as low as 10 m/s in the highest porosity materials, the clays. At the opposite extreme, the coarse sands with porosities around 0.4 show shear speeds in excess of 100 m/s. As with the compressional speed and attenuation, the shear-wave speed decays extremely rapidly in the coarse materials as the porosity increases slightly above its lowest value of 0.37. This behavior can be clearly seen in both the theoretical curve and the data. Because of the very high gradient at porosities in the vicinity of 0.4, a high-precision measurement of porosity would be required in order to predict accurately the speed of the shear wave in a sand sediment.

Figure 9(b) shows the shear attenuation as a function of porosity, with the smooth curve representing the prediction of the G-S theory [Eq. (4)]. Relatively few data points appear in Fig. 9(b), reflecting the difficulty of making *in situ* shear-attenuation measurements. Nevertheless, sufficient data are present to identify a lower bound to the effective attenuation, a boundary which is accurately traced by the intrinsic attenuation curve from the G-S theory. Apart from one errant point at  $N=0.63$ , the data lie on or above the theoretical line, again consistent with the idea that scattering and other loss mechanisms may add to the intrinsic attenuation predicted by the theory to yield the effective attenuation of the measurements.

## VIII. GRAIN-SIZE DEPENDENCE

### A. Compressional wave

Figure 10(a) shows the sound-speed ratio as a function of grain size, with the smooth curve representing the G-S theory [Eq. (1)]. The data are well distributed throughout the full range of grain sizes, from clays to coarse sands, and show a distinct upward trend with increasing grain size. The G-S theory follows the average trend of the data very satisfactorily.

The compressional attenuation as a function of the grain size is shown in Fig. 10(b), where the smooth curve represents the G-S theory [Eq. (2)], which was evaluated for a frequency of 38 kHz (i.e., the measurement frequency for much of the data) and divided by 38 to obtain dB/m/kHz. Throughout the range of grain sizes, from clays to coarse sands, the data points show a high degree of scatter as expected, since the data represent the effective attenuation. The

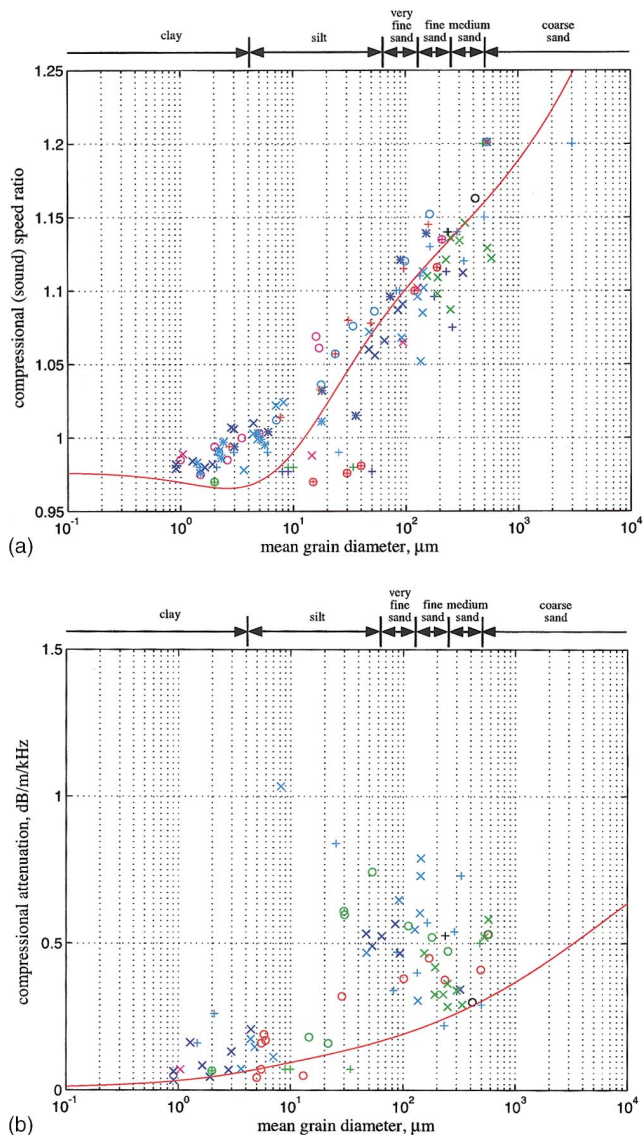


FIG. 10. (a) Sound-speed ratio versus mean grain diameter and (b) sound attenuation versus mean grain diameter. The red curves were evaluated from the G-S theory [Eqs. (1) and (2)] with  $f=38$  kHz and  $d=0.3$  m, and  $\Delta=1$   $\mu$ m in Eq. (17). To obtain the attenuation in dB/m/kHz, for comparison with the data, the value computed at 38 kHz was divided by 38. [Note: Hamilton's data have been included in these plots because the G-S theory and the experimental data indicate an insensitivity to the grain roughness parameter,  $\Delta$  that is, Hamilton's and Richardson's data follow much the same trend.]

lower boundary of the envelope occupied by the data is accurately traced by the theoretical curve computed from the G-S theory for the intrinsic attenuation.

### B. Shear wave

Data on shear-wave properties as a function of grain size are less abundant than those on the compressional wave. The shear speed versus mean grain diameter is plotted in Fig. 11(a), where the smooth curve represents the G-S theory [Eq. (3)] evaluated at a frequency of 1 kHz. Although a gap appears in the distribution of the data points between 15 and 40  $\mu$ m, a strong upward trend in the measured shear speed with increasing grain size is still easy to distinguish. Similar behavior is exhibited by the G-S theoretical curve.

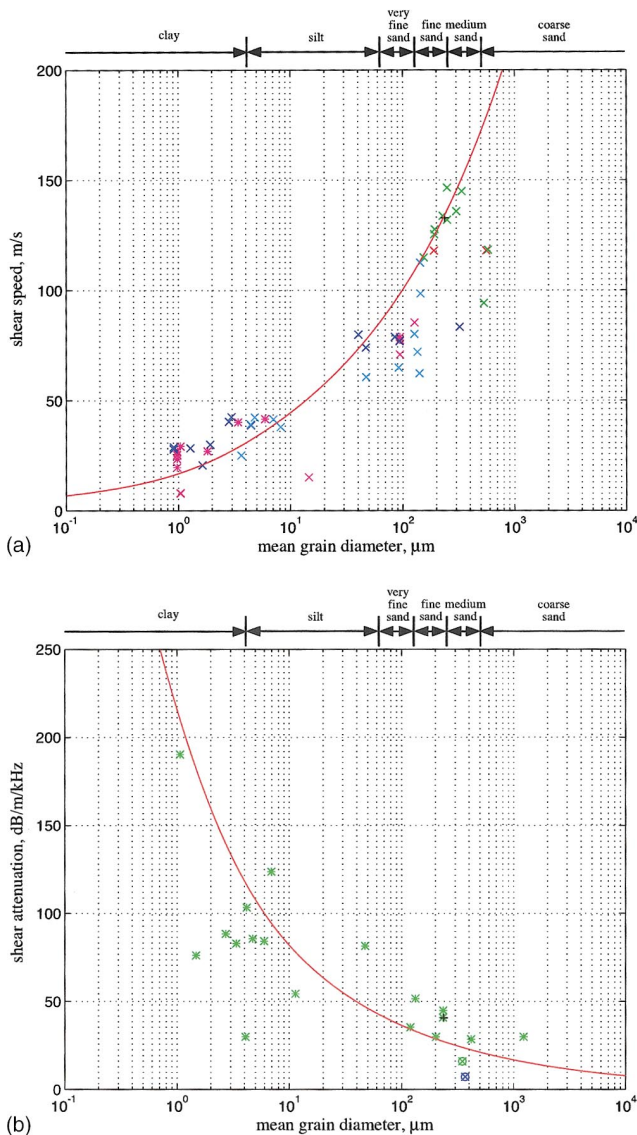


FIG. 11. (a) Shear-wave speed versus mean grain diameter and (b) shear-wave attenuation versus mean grain diameter. The red curves were evaluated from the G-S theory [Eqs. (3) and (4)] with  $f=1$  kHz and  $d=0.3$  m, and  $\Delta=1$   $\mu\text{m}$  in Eq. (17). [Note: The comment on Hamilton's shear wave data in the legend to Fig. 9 also applies here.]

As pointed out by Richardson,<sup>12</sup> shear attenuation has been measured at far fewer sites than shear speed. Those measurements of shear attenuation that are available are plotted in Fig. 11(b) against the mean grain diameter. The smooth curve in the diagram represents the G-S theory evaluated for a frequency of 1 kHz. Many of the data points fall close to or above the theoretical curve, again consistent with the idea that the data represent effective attenuation, the lower limiting value of which is the intrinsic attenuation yielded by the theory.

However, a group of data points in Fig. 11(b), representing very-fine-grained materials, silts and clays, with mean grain diameters in the range between 1 and 10  $\mu\text{m}$ , falls noticeably below the theoretical curve. It is not clear why these particular data points are seemingly too low (or the theoretical curve too high), especially as the very same measured values of shear attenuation lie above the theoretical curve in the plot of shear attenuation versus porosity in Fig.

9(b). The data points in question in Fig. 9(b) fall in the porosity range from approximately 0.55 to 0.6. In view of the extreme difficulty of making precision *in situ* measurements of shear attenuation in very-fine-grained sediments (shear speeds less than 50 m/s), the explanation for the apparently low data points in Fig. 11(b) may simply be a high level of uncertainty in these measurements. Since no error bars were reported with the original data set, it is difficult to ascertain whether this interpretation is plausible but the anomaly should be resolved, one way or the other, as more *in situ* shear-attenuation data become available.

## IX. A SHEAR-WAVE INVARIANT

If the product of the G-S expressions for the shear speed [Eq. (3)] and intrinsic attenuation [Eq. (4)] is formed, the resultant expression is

$$c_s \alpha_s = 2 \pi f \tan\left(\frac{n \pi}{4}\right) = 0.42f, \quad (20)$$

where  $f$  is frequency (Hz) and the value of  $n$  listed in Table II has been used to evaluate the scaling constant (0.42) on the right. According to Eq. (20), the product of the shear speed and attenuation is directly proportional to the frequency. The scaling constant is a function only of the strain-hardening coefficient  $n$ , being independent of all the macroscopic material properties of the sediment, that is, the porosity, the grain size, the density, and the overburden pressure. Since  $n$  represents microscopic processes occurring at grain contacts,<sup>17</sup> including strain hardening in the molecularly thin layer of fluid separating asperities, it is expected to be essentially constant for all sediments composed of similar materials, for instance, quartz grains and seawater. Thus, the constant 0.42 in Eq. (20) should hold for all siliclastic marine sediments

In principle, the predicted invariance of the shear speed times the shear attenuation provides a good test of the G-S theory. In practice, however, the number of sediment sites for which both shear-wave properties are available is almost vanishingly small, making such a test impracticable at present.

## X. CONCLUDING REMARKS

The properties of the phase speed and attenuation of compressional and shear waves in marine sediments have been examined in this article. Detailed comparisons have been made between measured wave properties, taken from the literature, and the predictions of a recently developed grain-shearing (G-S) theory of wave propagation in saturated porous media. The theory takes the form of two dispersion pairs, that is, four expressions, representing the phase speed and attenuation of the compressional wave and the shear wave. In addition to frequency, the four G-S dispersion relationships are functions of porosity, density, and grain size, and also overburden pressure, which translates into depth in the sediment.

Besides the material properties, the theoretical expressions involve three real parameters, representing microscopic shearing processes that are postulated to occur at grain con-

tacts during the passage of a wave. Two of these parameters, the compressional and shear coefficients, are analogous to the Lamé coefficients of elasticity theory, and the third is a numerical index representing the phenomenon of strain hardening in the molecularly thin layer of pore fluid sandwiched between grain contacts. Each of the three grain-shearing parameters has been assigned a value, which was held fixed in all the comparisons with data. Thus, the only available variables in the theoretical dispersion relationships are the material properties (porosity, grain size, and overburden pressure) and the frequency.

The compressional and shear-wave speeds and attenuations have been plotted as functions of frequency, depth in the sediment, porosity, and grain size, in each case with all other variables held constant. In every comparison, the theory accurately matches the average trend of the data set. It is to be emphasized that no adjustable parameters were available in the theory to help achieve these multiple fits to data.

The high quality of the match to data even holds for the attenuation of both the compressional and the shear wave: the theory reliably traces out the *lower bound* to the highly variable attenuation values returned by measurements. A straightforward interpretation of this observation is that the theory predicts the *intrinsic* attenuation, which arises from the irreversible conversion of wave energy into heat, whereas the measurements yield the *effective* attenuation, that is, the intrinsic attenuation plus any additional sources of loss, such as scattering from inhomogeneities in the granular medium. Since inclusions such as shell fragments tend to be randomly distributed in the sediment, the effective (i.e., measured) attenuation shows large fluctuations, taking values that are bounded from below by the intrinsic attenuation, which is stable and well predicted by the theory. In the plots of the compressional attenuation as a function of depth, for example, the theory accurately traces out the profile of the lowest attenuation values observed at each depth [Fig. 4(b)].

It is concluded that the G-S dispersion relationships in Eqs. (1) to (4), with the three fixed parameters  $\gamma_{po}$ ,  $\gamma_{so}$ , and  $n$  taking the values listed in Table I, are useful as a practical tool for making estimates of the wave and physical properties of a sediment (excluding the effective attenuation, of course, but including the intrinsic attenuation). For instance, if the sound speed were known, the shear speed, both (intrinsic) attenuations, the porosity, and the density could be evaluated immediately and uniquely from the G-S theoretical expressions. Similarly, if the porosity were available from, say, a core sample, the wave speeds and (intrinsic) attenuations could be evaluated from the G-S dispersion relations. Such utility has potential as the basis of a variety of inversion techniques for estimating the geoacoustic parameters of marine sediments.

## ACKNOWLEDGMENTS

Throughout the evolution of this work, Dr. Michael Richardson, NRL Stennis, has been generous with his sediment data as well as providing valuable guidance on the material properties of sediments. The research was supported by Dr. Ellen Livingston, Ocean Acoustics Code, the Office of Naval Research, under Grant Number N00014-04-1-0063.

- <sup>1</sup>E. L. Hamilton, G. Shumway, H. W. Menard, and C. J. Shipek, "Acoustic and other physical properties of shallow-water sediments off San Diego," *J. Acoust. Soc. Am.* **28**, 1–15 (1956).
- <sup>2</sup>E. L. Hamilton, H. P. Bucker, D. L. Keir, and J. A. Whitney, "Velocities of compressional and shear waves in marine sediments determined *in situ* from a research submersible," *J. Geophys. Res.* **75**, 4039–4049 (1970).
- <sup>3</sup>E. L. Hamilton, "Sound velocity and related properties of marine sediments, North Pacific," *J. Geophys. Res.* **75**, 4423–4446 (1970).
- <sup>4</sup>E. L. Hamilton, "Elastic properties of marine sediments," *J. Geophys. Res.* **76**, 579–604 (1971).
- <sup>5</sup>E. L. Hamilton, "Compressional-wave attenuation in marine sediments," *Geophysics* **37**, 620–646 (1972).
- <sup>6</sup>E. L. Hamilton, "Geoacoustic modeling of the sea floor," *J. Acoust. Soc. Am.* **68**, 1313–1336 (1980).
- <sup>7</sup>E. L. Hamilton and R. T. Bachman, "Sound velocity and related properties of marine sediments," *J. Acoust. Soc. Am.* **72**, 1891–1904 (1982).
- <sup>8</sup>E. L. Hamilton, "Acoustic properties of sediments," in *Acoustics and the Ocean Bottom*, edited by A. Lara-Saenz, C. Ranz Cuierra, and C. Carbo-Fité (Consejo Superior de Investigaciones Científicas, Madrid, 1987), pp. 3–58.
- <sup>9</sup>M. D. Richardson, E. Muzi, L. Troiano, and B. Miaschi, "Sediment shear waves: A comparison of *in situ* and laboratory measurements," in *Microstructure of Fine-Grained Sediments*, edited by R. H. Bennet, W. R. Bryant, and M. H. Hulbert (Springer, New York, 1991), pp. 403–415.
- <sup>10</sup>M. D. Richardson, E. Muzi, B. Miaschi, and F. Turgutcan, "Shear wave velocity gradients in near-surface marine sediment," in *Shear Waves in Marine Sediments*, edited by J. M. Hovem, M. D. Richardson, and R. D. Stoll (Kluwer, Dordrecht, 1991), pp. 295–304.
- <sup>11</sup>M. D. Richardson, "In-situ, shallow-water sediment geoacoustic properties," in *Shallow-Water Acoustics*, edited by R. Zhang and J. Zhou (China Ocean, Beijing, China, 1997), pp. 163–170.
- <sup>12</sup>M. D. Richardson, "Variability of shear wave speed and attenuation in surficial marine sediments," in *Impact of Littoral Environmental Variability on Acoustic Predictions and Sonar Performance*, edited by N. G. Pace and F. B. Jensen (Kluwer, La Spezia, 2002), pp. 107–114.
- <sup>13</sup>M. A. Biot, "Theory of propagation of elastic waves in a fluid-saturated porous solid. I. Low-frequency range," *J. Acoust. Soc. Am.* **28**, 168–178 (1956).
- <sup>14</sup>M. A. Biot, "Theory of propagation of elastic waves in a fluid-saturated porous solid. II. Higher frequency range," *J. Acoust. Soc. Am.* **28**, 179–191 (1956).
- <sup>15</sup>H. J. Simpson, B. H. Houston, S. W. Liskey, *et al.*, "At-sea measurements of sound penetration into sediments using a buried vertical synthetic array," *J. Acoust. Soc. Am.* **114**, 1281–1290 (2003).
- <sup>16</sup>E. L. Hamilton, "Sound velocity, elasticity, and related properties of marine sediments, North Pacific," Naval Undersea Research and Development Center, Report No. NUC TP 143 (1969).
- <sup>17</sup>M. J. Buckingham, "Wave propagation, stress relaxation, and grain-to-grain shearing in saturated, unconsolidated marine sediments," *J. Acoust. Soc. Am.* **108**, 2796–2815 (2000).
- <sup>18</sup>A. B. Wood, *A Textbook of Sound*, 3rd ed. (Bell, London, 1964).
- <sup>19</sup>S. P. Timoshenko and J. N. Goodier, *Theory of Elasticity*, 3rd ed. (McGraw-Hill, New York, 1970).
- <sup>20</sup>E. L. Hamilton, "Shear-wave velocity versus depth in marine sediments: A review," *Geophysics* **41**, 985–996 (1976).
- <sup>21</sup>R. D. Stoll, *Sediment Acoustics* (Springer, Berlin, 1989).
- <sup>22</sup>M. D. Richardson and K. B. Briggs, "In situ and laboratory geoacoustic measurements in soft mud and hard-packed sand sediments: Implications for high-frequency acoustic propagation and scattering," *Geo-Mar. Lett.* **16**, 196–203 (1996).
- <sup>23</sup>M. J. Buckingham and M. D. Richardson, "On tone-burst measurements of sound speed and attenuation in sandy marine sediments," *IEEE J. Ocean. Eng.* **27**, 429–453 (2002).
- <sup>24</sup>M. D. Richardson, D. L. Lavoie, and K. B. Briggs, "Geoacoustic and physical properties of carbonate sediments of the Lower Florida Keys," *Geo-Mar. Lett.* **17**, 316–324 (1997).
- <sup>25</sup>M. D. Richardson, K. B. Briggs, D. L. Bibee *et al.*, "Overview of SAX99: Environmental considerations," *IEEE J. Ocean. Eng.* **26**, 26–53 (2001).
- <sup>26</sup>F. Collins and C. C. Lee, "Seismic wave attenuation characteristics," *Geophysics* **21**, 16–40 (1956).
- <sup>27</sup>L. Knopoff and G. J. F. MacDonald, "The attenuation of small amplitude stress waves in solids," *Rev. Mod. Phys.* **30**, 1178–1192 (1958).
- <sup>28</sup>W. I. Futterman, "Dispersive body waves," *J. Geophys. Res.* **67**, 5279–5291 (1962).

- <sup>29</sup>K. L. Williams, "An effective density fluid model for acoustic propagation in sediments derived from Biot theory," *J. Acoust. Soc. Am.* **110**, 2276–2281 (2001).
- <sup>30</sup>K. L. Williams, D. R. Jackson, E. I. Thorsos, , "Comparison of sound speed and attenuation measured in a sandy sediment to predictions based on the Biot theory of porous media," *IEEE J. Ocean. Eng.* **27**, 413–428 (2002).
- <sup>31</sup>M. J. Buckingham, "A three-parameter dispersion relationship for Biot's fast compressional wave in a marine sediment," *J. Acoust. Soc. Am.* **116**, 769–776 (2004).
- <sup>32</sup>H. J. Simpson and B. H. Houston, "Synthetic array measurements of acoustical waves propagating into a water-saturated sandy bottom for a smoothed and a roughened interface," *J. Acoust. Soc. Am.* **107**, 2329–2337 (2000).
- <sup>33</sup>Michael D. Richardson, personal communication, Feb. 2000.
- <sup>34</sup>E. L. Hamilton, "Sound velocity gradients in marine sediments," *J. Acoust. Soc. Am.* **65**, 909–922 (1979).
- <sup>35</sup>E. L. Hamilton, "Sound velocity as a function of depth in marine sediments," *J. Acoust. Soc. Am.* **78**, 1348–1355 (1985).
- <sup>36</sup>E. L. Hamilton, "Sound attenuation as a function of depth in the sea floor," *J. Acoust. Soc. Am.* **59**, 528–535 (1976).
- <sup>37</sup>G. H. F. Gardner, M. R. J. Wyllie, and D. M. Droschak, "Effects of pressure and fluid saturation on the attenuation of elastic waves in sands," *J. Pet. Technol.* **16**, 189–198 (1964).
- <sup>38</sup>A. N. Hunter, R. Legge, and E. Matsukawa, "Measurements of acoustic attenuation and velocity in sand," *Acustica* **11**, 26–31 (1961).
- <sup>39</sup>R. A. Wheatcroft, "*In situ* measurements of near-surface porosity in shallow-water marine sands," *IEEE J. Ocean. Eng.* **27**, 561–570 (2002).
- <sup>40</sup>O. K. Rice, "On the statistical mechanics of liquids, and the gas of hard elastic spheres," *J. Chem. Phys.* **12**, 1–18 (1944).
- <sup>41</sup>M. R. Wyllie, A. R. Gregory, and L. W. Gardner, "Elastic wave velocities in heterogeneous and porous media," *Geophysics* **21**, 41–70 (1956).
- <sup>42</sup>M. J. Buckingham, "Theory of acoustic attenuation, dispersion, and pulse propagation in unconsolidated granular materials including marine sediments," *J. Acoust. Soc. Am.* **102**, 2579–2596 (1997).
- <sup>43</sup>E. L. Hamilton, "Sediment sound velocity measurement made *in-situ* from bathyscaph *Trieste*," *J. Geophys. Res.* **68**, 5991–5998 (1963).
- <sup>44</sup>E. L. Hamilton, "Low sound velocities in high-porosity sediments," *J. Acoust. Soc. Am.* **28**, 16–19 (1956).
- <sup>45</sup>A. B. Wood and D. E. Weston, "The propagation of sound in mud," *Acustica* **14**, 156–162 (1964).
- <sup>46</sup>M. D. Richardson, "Spatial variability of surficial shallow water sediment geoaoustic properties," in *Ocean-Seismo Acoustics: Low-Frequency Underwater Acoustics*, edited by T. Akal and J. M. Berkson (Plenum, New York, 1986), pp. 527–536.
- <sup>47</sup>B. A. Brunson and R. K. Johnson, "Laboratory measurements of shear wave attenuation in saturated sand," *J. Acoust. Soc. Am.* **68**, 1371–1375 (1980).
- <sup>48</sup>B. A. Brunson, "Shear wave attenuation in unconsolidated laboratory sediments," in *Shear Waves in Marine Sediments*, edited by J. M. Hovem, M. D. Richardson, and R. D. Stoll (Kluwer, Dordrecht, 1991), pp. 141–147.
- <sup>49</sup>M. D. Richardson and K. B. Briggs, "On the use of acoustic impedance values to determine sediment properties," in *Acoustic Classification and Mapping of the Seabed*, edited by N. G. Pace and D. N. Langhorne (University of Bath, Bath, 1993), Vol. 15, pp. 15–24.
- <sup>50</sup>E. G. McLeroy and A. DeLoach, "Sound speed and attenuation, from 15 to 1500 kHz, measured in natural sea-floor sediments," *J. Acoust. Soc. Am.* **44**, 1148–1150 (1968).
- <sup>51</sup>C. McCann and D. M. McCann, "The attenuation of compressional waves in marine sediments," *Geophysics* **34**(6), 882–892 (1969).
- <sup>52</sup>G. W. C. Kaye and T. H. Laby, *Tables of Physical and Chemical Constants and Some Mathematical Functions*, 12th ed. (Longmans Green and Co., London, 1959).
- <sup>53</sup>M. D. Richardson, K. L. Williams, K. B. Briggs, and E. I. Thorsos, "Dynamic measurement of sediment grain compressibility at atmospheric pressure: Acoustic applications," *IEEE J. Ocean. Eng.* **27**, 593–601 (2002).